Self-aligned local contact opening and n+ diffusion by single-step laser doping from POx/Al2O3 passivation stacks

Solar Energy Materials & Solar Cells 217 (2020) 110717

Contents lists available at ScienceDirect

Solar Energy Materials and Solar Cells

journal homepage: http://www.elsevier.com/locate/solmat

Self-aligned local contact opening and $n+$ diffusion by single-step laser doping from PO_x/Al_2O_3 passivation stacks

Lachlan E. Black [a,*], Marco Ernst [a,**], Roel Theeuwes [b], Jimmy Melskens [b], Daniel Macdonald [a], W.M.M.(Erwin) Kessels [b]

[a] Research School of Electrical, Energy and Materials Engineering, ANU College of Engineering and Computer Science, Building 31, The Australian National University, Canberra ACT, 2600, Australia

[b] Department of Applied Physics, Eindhoven University of Technology, P.O. Box 513, 5600, MB Eindhoven, the Netherlands

ARTICLE INFO

Handling Editor: Ivan Gordon

Keywords:
Laser-doping
Surface passivation
Phosphorus oxide
Aluminium oxide
Silicon solar cells

ABSTRACT

Laser doping is a promising route to realise industrially compatible processing of local contacts for high-efficiency solar cells, especially when the same film acts as both dopant source and passivation layer. In this work we demonstrate simultaneous local contact opening and $n+$ laser doping of silicon from positively charged PO_x/Al_2O_3 thin-film stacks, which also provide outstanding passivation of n-type silicon surfaces. Local $n+$ doped regions with sheet resistance ranging from 35 to ~540 Ω/□ are formed using single nanosecond laser pulses with varying fluence. ECV profiling shows net n-type doping in all cases, confirmed by SIMS profiling to be due to phosphorus from the PO_x layer. J_0 of metallised laser-doped regions is consistent with values achieved for state-of-the-art furnace diffusions with similar sheet resistance, confirming that laser-induced recombination-active defects are avoided. A minimum J_0 of 540 fA cm^{-2} is obtained for metallised laser-doped regions formed from PO_x/Al_2O_3 passivation stacks having J_0 of 2.5 fA cm^{-2}. The combination of outstanding passivation of uncontacted n-type regions offered by PO_x/Al_2O_3, with self-aligned formation of locally-diffused contact openings via single-step laser processing, opens up exciting possibilities for simplified fabrication of high-efficiency cell structures.

1. Introduction

High-efficiency crystalline silicon solar cell concepts such as PERL (passivated emitter and rear locally diffused) and IBC (interdigitated back contact), which utilise local contacts to reduce contact recombination, have demonstrated some of the highest efficiencies in laboratory devices [1,2]. Transferring such technologies to industry requires substituting complex photolithographic patterning with low-cost, high-throughput processes for local contact formation. Laser-based processing has emerged as the preferred solution for this problem [3,4].

Current industrial p-type PERC cells achieve local contact opening via laser ablation of the rear dielectric, followed by screen-printing and firing of Al paste to form local $p+$ Al "back surface field" (Al-BSF) contacts. This significantly reduces rear-side recombination compared with a conventional full-area Al-BSF. However, owing to the mechanics of Al-BSF formation, this process limits the minimum contact fraction that can be achieved while maintaining low contact recombination when using standard Al pastes, or requires the use of Al pastes with a high Si content, which increases series resistance [5]. Furthermore, while the highest laboratory efficiencies have been achieved on n-type silicon, there is no analogous process available for n-type local contact formation, which is a barrier to adoption of n-type PERC technology.

An alternative to Al-BSF formation is the use of laser processing to achieve local diffusion of dopants from thin-film sources. Laser doping of P or B has been realised from a variety of such sources, including furnace-grown phosphosilicate glass (PSG) [6–8] and borosilicate glass (BSG) [9], doped CVD SiO_x [10], and various spin-on films [11,12]. Such sources are generally sacrificial and must be removed after laser-processing to allow deposition of a separate surface passivation layer.

A particularly elegant process simplification is possible when the thin-film dopant source also acts as passivation layer. In this case, it becomes possible to realise simultaneous local opening of the passivation layer and self-aligned dopant diffusion in a single process step,

* Corresponding author.
** Corresponding author.
E-mail addresses: lachlan.black@anu.edu.au (L.E. Black), marco.ernst@anu.edu.au (M. Ernst).

https://doi.org/10.1016/j.solmat.2020.110717
Received 1 June 2020; Received in revised form 21 July 2020; Accepted 23 July 2020
Available online 18 August 2020

thereby eliminating additional etching, deposition, and alignment steps. For *p*-type doping, Al_2O_3 has attracted significant attention as a highly-effective passivation layer able to act as a dopant source for laser doping, either alone [13,14] or in stacks with PECVD SiN_x [15–17] or SiC_x [18,19], while *p*-type laser doping has also been realised from passivating Ga_2O_3 [20], as well as stacks of Al_2O_3 and B-doped a-SiC_x [21] or SiN_x [22,23].

In the case of *n*-type laser doping, P-doped a-SiC_x [24,25] and SiN_x [22,26,27] have been investigated as passivating dopant sources. However, the relatively low P content in such layers limits the achievable surface dopant concentration to around 10^{19} cm^{-3}, with consequences for contact resistance and the effectiveness of minority carrier screening.

PO_x/Al_2O_3 dielectric stacks have recently been demonstrated as highly effective passivation layers for *n*-type silicon surfaces [28,29], thanks to an unusually large positive fixed charge and low interface state density, with passivation comparable to or better than state-of-the-art PECVD SiN_x:H [29,30]. Since P and Al are respectively *n*- and *p*-type dopants in silicon, such stacks are obvious candidates as dopant sources for laser doping. An important question is whether the presence of both dopants results in significant compensation and whether the resulting net doping is *p*- or *n*-type. In this contribution we investigate the suitability of such stacks for laser doping and estimate their efficiency potential in commercial *n*-type PERL solar cells.

2. Materials and methods

Samples for sheet resistance, dopant profiling, and lifetime measurements were prepared on high-resistivity (~50 Ω cm) planar (100) *n*-type FZ Si wafers (~315 μm thickness). These received a Tabula Rasa treatment at 1000 °C in oxygen atmosphere to dissolve oxygen precipitates, followed by removal of SiO_2 in HF and a standard Radio Corporation of America (RCA) clean.

PO_x/Al_2O_3 stacks of varying thickness (3–6 nm for the PO_x layer, and 11–15 nm for Al_2O_3) were deposited in an ALD reactor (Oxford Instruments FlexAL) at 100 °C. PO_x was deposited from trimethyl phosphate (TMPO) and O_2 plasma, and Al_2O_3 from trimethyl aluminium (TMA) and O_2 plasma [28]. Wafers received an HF dip (1% HF, 1 min) and DI water rinse to remove the RCA oxide immediately prior to loading in the ALD system. The thickness of the films was monitored by in-situ spectroscopic ellipsometry (J. A. Woollam M2000). Following deposition, samples were annealed at 400 °C in N_2 for 10 min in a tube furnace to activate the passivation.

Laser processing was performed using a 248 nm excimer laser with pulse duration of ~25 ns at a range of fluences. Larger regions were patterned by rastering pulses of a 500 × 500 μm^2 flat-top beam with a 2% beam overlap. In some cases, pulses were repeated multiple times to further vary obtained dopant profiles.

Sheet resistance was measured on 12 mm × 2 mm laser-processed regions by four-point probe, using geometric correction factors taken from Ref. [31]. The small contribution of the *n*-type wafer bulk was subtracted from the measured total sheet conductance values. Net active dopant concentration profiles were measured by electrochemical capacitance–voltage (ECV) profiling (WEP Wafer Profiler CVP21). Measured profiles were corrected based on the actual etch area as measured using a digital optical microscope. Commercial SIMS measurements were performed by EAG Laboratories.

Saturation current density J_0 of laser-processed regions was determined using photoluminescence (PL) imaging of wafers symmetrically passivated by PO_x/Al_2O_3 stacks, with arrays of 13 mm × 13 mm laser-processed regions formed on the rear side using a range of laser settings. PL imaging (BT Imaging LIS-R1) was performed at a range of excitation levels using a black back-sheet to suppress rear-side reflection of the excitation source. Smearing of the PL signal between low- and high-lifetime regions was corrected by deconvolution of the raw PL images using the experimentally determined point-spread function of the system [32]. Deconvolution was performed using the regularized Richardson–Lucy algorithm as implemented in the freely available ImageJ plugin, Deconvolution Lab [33]. The number of iterations used (20) was chosen to achieve saturation of the deconvolved intensities for all regions.

Excess carrier concentration Δn and effective lifetime τ_{eff} were determined from the deconvolved PL intensity I_{PL} of each region according to

$$\Delta n^2 = C I_{PL}$$

$$\tau_{eff} = \Delta n / G_{av}$$

where C is a constant of proportionality and G_{av} is the average generation rate, given by $G_{av} = \Phi A_{opt}/W$, with the (known) photon flux Φ, wafer thickness W, and $0 \leq A_{opt} \leq 1$ the fraction of incident photons absorbed by the wafer. We use $A_{opt} = 0.7$, based on optical simulations of our samples. Given A_{opt}, C was determined by calibrating the resulting values for $\tau_{eff}(\Delta n)$ for the unprocessed (symmetrically passivated) regions against transient photoconductance lifetime measurements of the same regions (Sinton Instruments WCT-120 [34]). J_0 was determined via the method of Kane and Swanson [35] from measurements at a range of excitation levels, using the intrinsic lifetime parameterisation of Richter et al. [36], and intrinsic carrier concentration $n_i = 8.6 \times 10^9$ cm^{-3} ([37] at 25 °C). Note that the precise value of A_{opt} is not critical for J_0 determination by this method, since changes in A_{opt} are compensated by changes in C such that the slope of τ_{eff}^{-1} vs Δn is approximately maintained.

3. Results and discussion

Initial experiments were performed on two film stacks with varying PO_x thickness (3 nm or 6 nm) and fixed 15 nm Al_2O_3 capping layer thickness. Single-pulse laser processing was performed with fluences ranging from 0.75 to 2.75 J cm^{-2}. Sheet resistances ranging from ~400 to 35 Ω/□, depending on laser fluence and PO_x thickness, were obtained after laser-processing (Fig. 1a), indicating significant dopant incorporation. ECV profiling (Fig. 1b) showed net *n*-type doping in all cases, with active surface dopant concentrations ranging from ~4×10^{19} to ~5×10^{20} cm^{-3}. For the samples with 6 nm PO_x thickness we observe a trend of decreasing sheet resistance with laser fluence, consistent with the increased depth and concentration of the ECV profiles, saturating at ~35 Ω/□ for laser fluences above 1.5 J cm^{-2}. We explain the peak at 1 J cm^{-2} for the stack with 6 nm PO_x by a possible compensation of the *p*- and *n*-type dopants. The samples with 3 nm PO_x thickness show an opposite trend of increasing sheet resistance with fluence, also saturating (at ~90 Ω/□) for fluences above 1.5 J cm^{-2}. The reason for this trend with fluence is not clear (the ECV data suggests an opposite trend), although the saturation at a higher sheet resistance for the thinner PO_x layer is consistent with the reduced quantity of P available from the latter.

SIMS profiling of two of the regions, processed from 6 nm/15 nm PO_x/Al_2O_3 stacks with two different laser fluences (Fig. 2a), confirms that doping is due to P from the PO_x layer, while Al from the Al_2O_3 capping layer is concentrated near the surface and apparently inactive. Relatively narrow high-concentration Al and P surface peaks are combined with a deeper P tail with a peak concentration consistent with the active peak concentration measured by ECV. The shape of this P tail is well-described by an offset Gaussian function. The Al tail is much

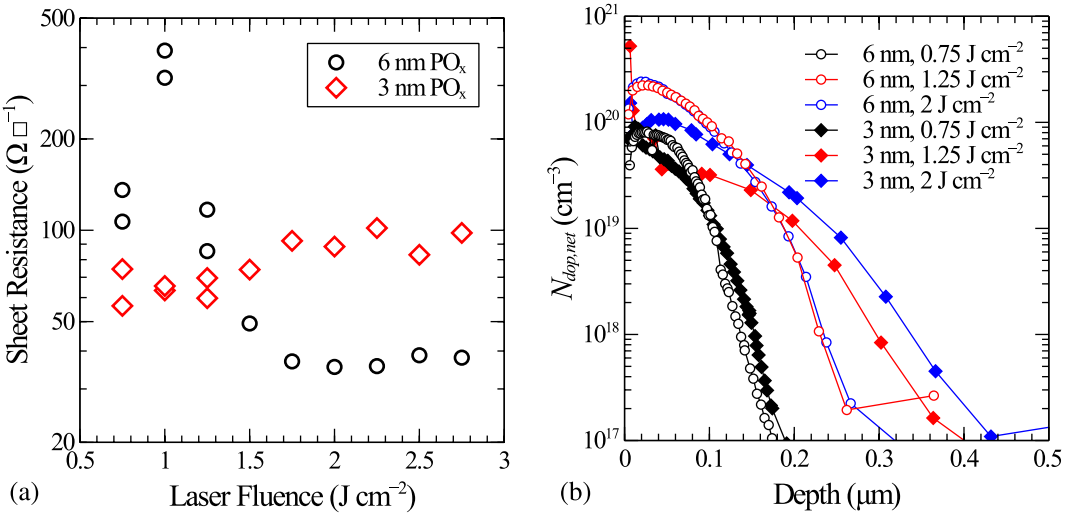

Fig. 1. a) Sheet resistance vs laser fluence for laser-doped regions formed from 6 nm/15 nm and 3 nm/15 nm PO_x/Al_2O_3 stacks. b) Active net dopant concentration profiles measured by ECV for the same samples at several laser fluences. The net doping is *n*-type in all cases.

weaker and exhibits a roughly exponential decay.

Since the high Al and P concentrations in the near-surface peaks is not reflected in the active dopant profiles, the majority of these atoms are presumably not active as dopants. The fact that the higher Al concentration near the surface also does not result in net *p*-type doping also indicates that the Al, if active at all, becomes so at a lower concentration threshold than the P. The concentration of Al and P atoms in these surface peaks is actually so high that if the surrounding matrix is assumed to be crystalline silicon (atomic density 5×10^{22} cm^{-3}) they would represent peak concentrations of 20–29% and 6.3–7.3% respectively. An alternative possibility is that they instead represent Al and P in remnant surface oxides (SIMS measurements of oxygen concentration were not performed). We note however, that we had no difficulty performing ECV and four-point probe measurements on the same samples without further treatment. Further work is required to understand and possibly influence the behaviour of the involved materials during laser doping from such stacks.

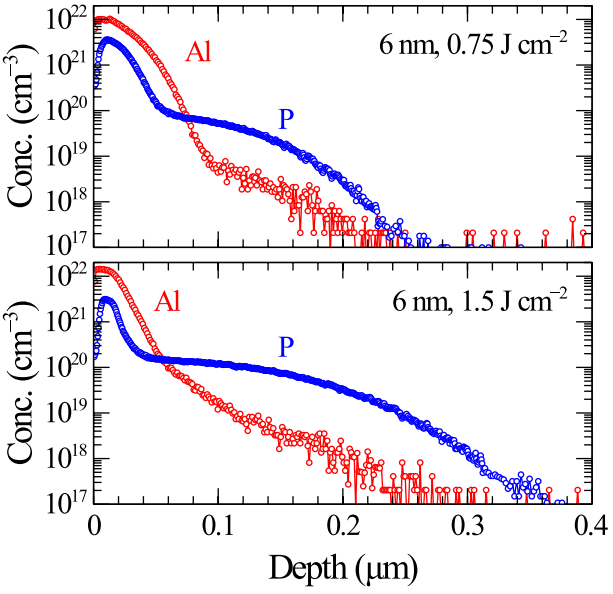

Fig. 2. Al and P concentrations measured by SIMS profiling after laser-doping from 6 nm/15 nm PO_x/Al_2O_3 stacks at fluences of 0.75 and 1.5 J cm^{-2}.

In order to obtain information about the recombination in such laser-processed regions, a second set of samples were symmetrically passivated with a 4.5 nm/11 nm PO_x/Al_2O_3 stack optimised for its passivation properties. An array of 13 mm × 13 mm laser-doped regions was processed on one side using laser fluences of 0.5–2 J cm^{-2} and 1–6 pulse repetitions. A full-area 5 nm Al metal layer was thermally evaporated on the same side in order to induce the effectively infinite surface recombination velocities found at a metallised surface. J_0 was determined from PL imaging at a range of excitation levels as described in Section 2. Deconvolution of the PL images (Fig. 3) was found to be essential to recover the contrast between high and low PL intensity regions in order

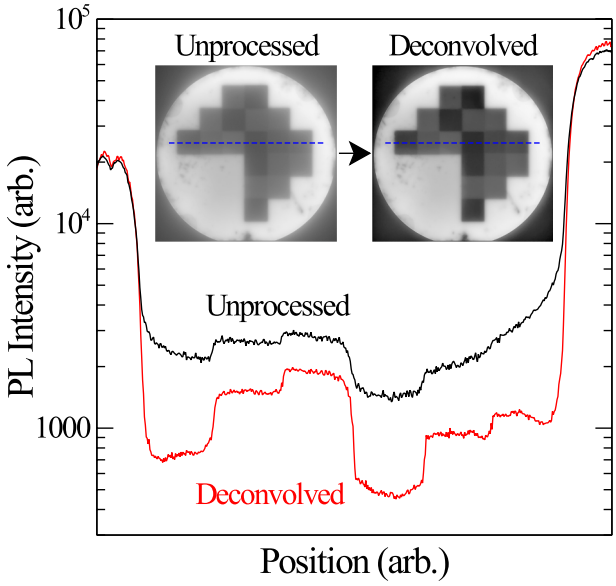

Fig. 3. Example of PL image deconvolution for a laser-processed sample. The sample is a 50 Ω cm *n*-type FZ Si wafer symmetrically passivated by 4.5 nm/11 nm PO_x/Al_2O_3 stacks, with an array of square-shaped laser-doped regions on the rear side, processed with a range of laser settings, and a full-area rear metallisation (5 nm Al evaporation). Insets show the unprocessed PL image, and the same image following deconvolution using the point-spread function of the imaging system [38] (images shown using the same log scale). The main plot shows corresponding line profiles (dashed lines in insets) of PL intensity for the unprocessed and deconvolved images.

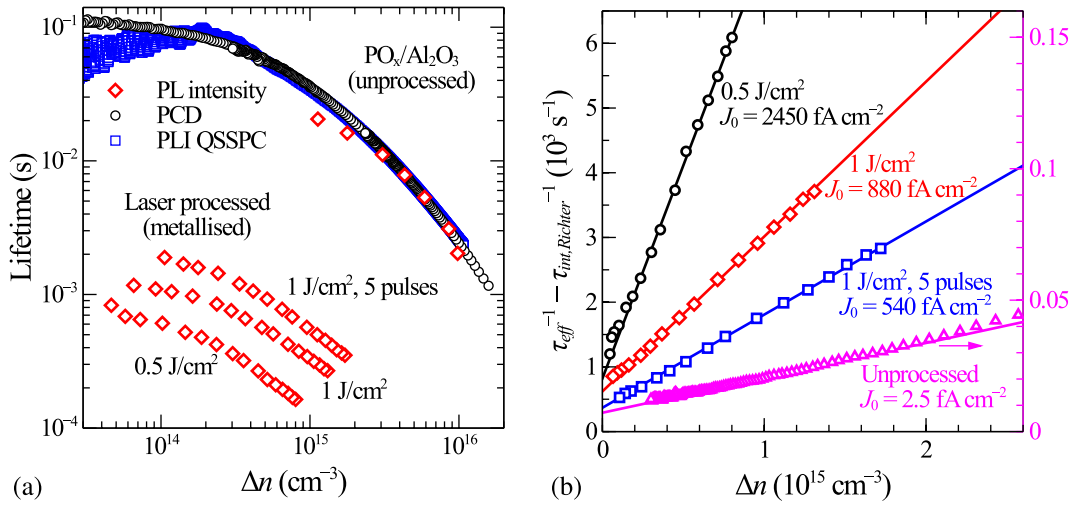

Fig. 4. a) Carrier lifetime versus excess carrier concentration for 50 Ω cm *n*-type FZ Si wafer symmetrically passivated by a 4.5 nm/11 nm PO_x/Al_2O_3 stack, measured by transient PCD using a Sinton WCT-120 lifetime tester and by QSSPC in a PL imaging system. Values determined from PL intensity imaging of the same sample before and after laser processing and metallisation with different laser fluences are also shown, calibrated against the PCD values. b) Illustration of J_0 extraction via the method of Kane and Swanson for metallised laser-doped regions processed with different laser settings, using the lifetimes determined from the PL intensity. The extraction of J_0 from the PCD data for the unprocessed PO_x/Al_2O_3 passivated sample is also shown, using a separate vertical scale.

to avoid underestimation of J_0, especially for high recombination regions.

The resulting $\tau_{eff}(\Delta n)$ extracted for laser-doped regions processed with several settings is shown in Fig. 4a, together with values determined for the unprocessed sample by the same method and via photoconductance measurements. The outstanding passivation provided by the unprocessed PO_x/Al_2O_3 passivation stack results in τ_{eff} as high as 110 ms for this sample in low injection (corresponding to $S_{eff,max} < 0.15$ cm/s, assuming infinite bulk lifetime), and 36.3 ms at $\Delta n = 10^{15}$ cm^{-3}. A J_0 of 2.5 fA cm^{-2} per side was measured by the method of Kane and Swanson (Fig. 4b). Fig. 4b also shows extraction of J_0 for the laser-processed regions. The excellent linear behaviour of the corrected inverse lifetime resulting from the PL intensity measurements provides confidence that the extracted J_0 values are reliable.

Fig. 5 shows the resulting J_0 values as a function of the number of laser pulse repetitions at various laser fluences, along with the corresponding sheet resistances R_{sheet} measured by four-point probe. The J_0 values range from 2450 to 540 fA cm^{-2}, and are clearly correlated with the sheet resistance values, which range from ~540 to 39.5 Ω/□. This correlation is expected due to improved screening of minority carriers from the metallised surface with increased depth and concentration of the dopant profile. In general, there is a trend of decreasing J_0 and R_{sheet} with increasing pulse count after the second pulse, although both are lower for one pulse than for two at the higher fluences. The lowest J_0 of 540 fA cm^{-2} was obtained for five pulse repetitions at a fluence of 1 J cm^{-2}. The corresponding R_{sheet} was 39.5 Ω/□, which was also the lowest value measured for these samples. The lowest J_0 obtained using a single pulse was 700 fA cm^{-2} (R_{sheet} = 46 Ω/□), at a fluence of 1.5 J cm^{-2}.

Fig. 6 shows the corresponding ECV profiles measured for the 4.5 nm/11 nm PO_x/Al_2O_3 stacks processed with fluences of 1, 1.5 and 2 J cm^{-2} with 1, 2 and 5 pulses (5 pulses at 2 J cm^{-2} was not tested). Measurements of areas processed with fluences of 0.5 J cm^{-2} were also attempted but could not be completed due to too high contact resistance. All profiles were again found to be net *n*-type. As expected from the similar J_0 and R_{sheet} values obtained, the profiles following single-pulse laser processing are similar for the three fluences examined. However, significant differences in profile shape and peak concentration emerge following the second and subsequent pulses, depending on the fluence, which presumably account for the differences in J_0 and R_{sheet} for pulse

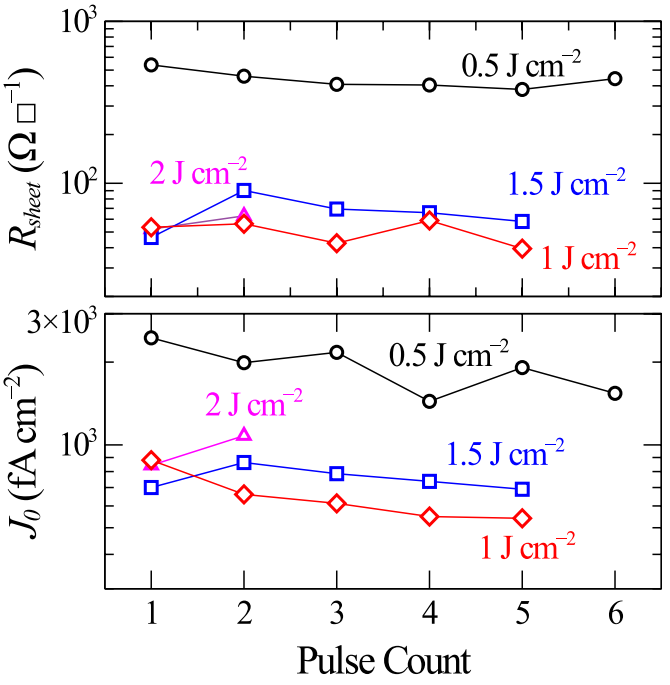

Fig. 5. Sheet resistance R_{sheet} and saturation current density J_0 (after metallisation) for laser-doped regions formed from 4.5 nm/11 nm PO_x/Al_2O_3 stacks using various laser fluences as a function of the number of laser pulses.

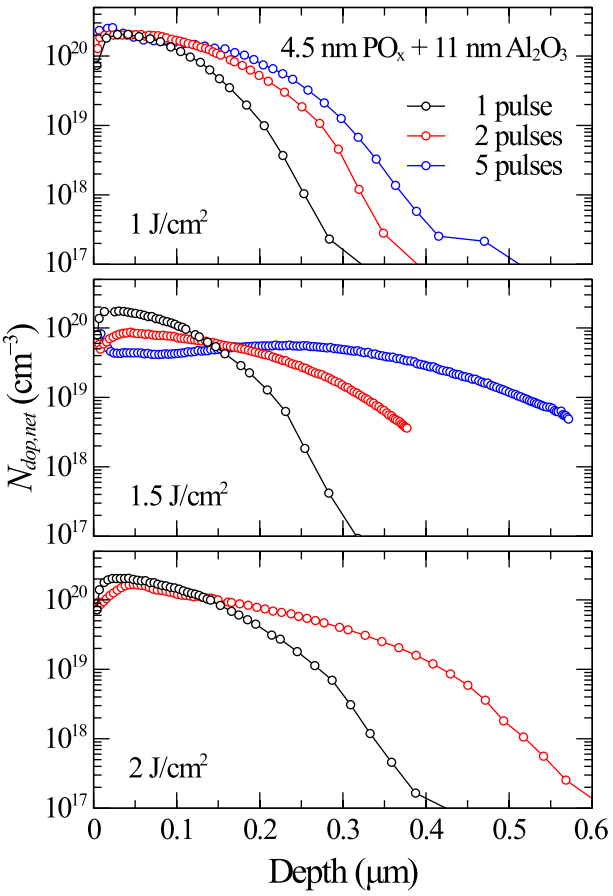

Fig. 6. Active net dopant concentration profiles measured by ECV after laser doping from 4.5 nm/11 nm PO_x/Al_2O_3 stacks at various laser fluences as a function of the number of laser pulses.

count ≥2 shown in Fig. 5. This indicates that laser fluence and pulse count have a significant influence on final dopant profile, which in turn provides opportunities for tuning these to achieve desired properties.

Despite these differences, a general trend of increasing profile depth and decreasing surface concentration is apparent with increasing pulse count. This is analogous to the effect of a drive-in step following a furnace diffusion. The profile following 5 pulses at 1.5 J cm^{-2} shows the most significant changes, including the appearance of a pronounced dip in the near-surface region. This is inconsistent with surface depletion and may actually be evidence of significant Al co-doping in this range.

The correlation of J_0 with R_{sheet} apparent in Fig. 5 is consistent with previous reports for metallised $n+$ regions. In Fig. 7 we plot these values against each other, together with values previously reported [39] for $POCl_3$ furnace diffusions (adjusted to $n_i = 8.6 \times 10^9$ cm^{-3}). J_0 values for metallised laser-processed regions are clearly consistent with those for furnace diffusions with similar sheet resistances. This indicates that laser processing does not introduce significant recombination-active defects in this case, which is unlike what has been reported to be the case for laser-doping from Al_2O_3 in particular [14].

In order to estimate the potential efficiency gains from PO_x/Al_2O_3 stacks as passivation and dopant source for laser contact formation, we perform device simulations in Quokka3 [40] of commercial n-type PERT/PERL solar cells (using same n_i and Auger models used for J_0 extraction). Our starting point is a commercial n-type front-emitter PERT solar cell, built on parameters published in Refs. [41–43]. We

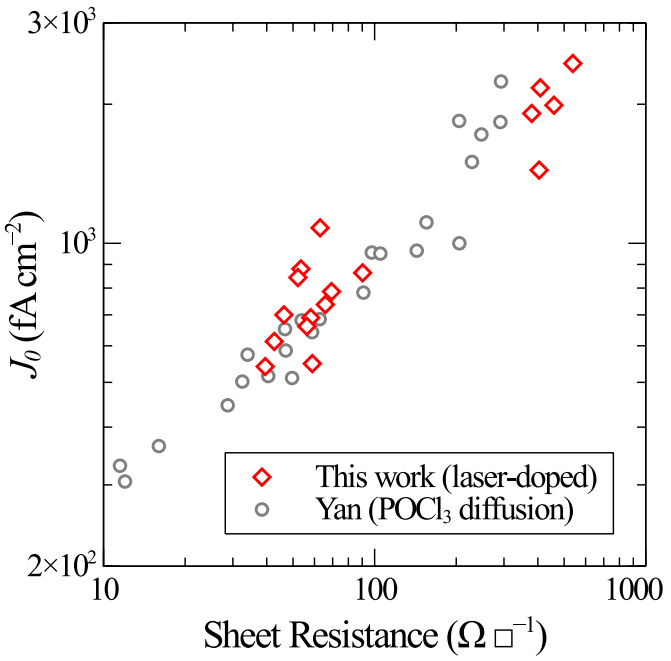

Fig. 7. Surface saturation current density J_0 vs sheet resistance for metallised laser-doped regions processed from 4.5 nm/11 nm PO_x/Al_2O_3 stacks with a range of laser settings. Also shown are values reported by Yan and Cuevas [39] for metallised $POCl_3$ furnace diffusions with various drive-ins.

assume improved front-side passivation and contacting ($J_{0,pass,front} = 15$ fA cm^{-2}, $J_{0,c,front} = 600$ fA cm^{-2}, $\rho_{c,front} = 1$ mΩ cm^2), and bulk lifetime (8 ms) following the efficiency roadmap for industrial front-emitter n-type PERT solar cells outlined in Ref. [43]. We apply the PO_x/Al_2O_3 passivation stack ($J_0 = 2.5$ fA cm^{-2}) to the planar rear surface, replacing the typical SiN_x film, together with a light (500 Ω/□) full-area $n+$ rear diffusion to assist with lateral transport. The latter raises total recombination at the passivated rear surface just slightly to $J_{0,pass,rear} = 4$ fA cm^{-2} (as simulated by EDNA2 [44]). We implement locally laser-doped line contacts from the PO_x/Al_2O_3 stack (thus resulting in an analogous structure to industrial p-type PERC solar cells). We optimise the width and pitch of the line-shaped localised contacts, allowing a minimum contact width of 20 μm in accordance with realistic limits for industrial laser processes.

Fig. 8 shows the resulting device efficiency as a function of the local rear contact resistivity $\rho_{c,rear}$ and contact recombination $J_{0,c,rear}$, with an optimised contact fraction of the line shaped contacts at each combination of $J_{0,c,rear}$ and $\rho_{c,rear}$. In this optimisation the pitch and contact width were limited to a minimum of 600 μm and 20 μm, respectively. The red star indicates the estimated efficiency of 23.59% ($V_{oc} = 701$ mV, $J_{sc} = 41.1$ mA cm^{-2}, $FF = 81.77\%$), based on the measured contact recombination of 540 fA cm^{-2} achieved for metallised laser contacts in this work, and a contact resistivity of 0.1 mΩ cm^2 [12]. We note that previous work [45] indicates a negligible dependence of the contact recombination on the contact size for the laser fluence applied in this paper. At such low contact recombination values, we find a negligible sensitivity to the contact resistivity, enabling device efficiency exceeding 23.5% even at values one order of magnitude higher than previously achieved for localised laser-doped contacts.

The optimised efficiency of 23.59% is obtained using a rear contact fraction of 2.5% (line contacts with 20 μm width, 800 μm pitch). This results in a total area-weighted J_0 of just 15.9 fA cm^{-2} for the rear side (including both passivated and contacted regions). The free-energy loss

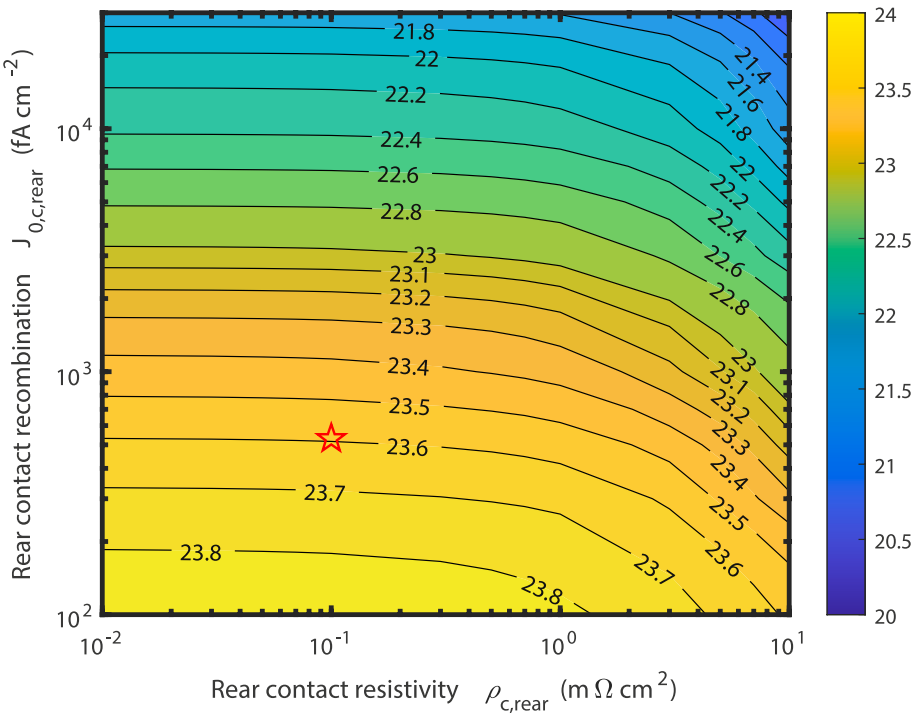

Fig. 8. Contour plot of simulated (Quokka3) efficiency for a commercial n-type PERL solar cell with PO_x/Al_2O_3 rear surface passivation and laser-doped line contacts, as a function of rear contact recombination $J_{0,c,rear}$ and contact resistivity $\rho_{c,rear}$. Cell parameters are based on those published in Ref. [41–43], incorporating previously roadmapped [43] improvements to front side passivation and bulk lifetime. The contact fraction is optimised for each combination of $J_{0,c,rear}$ and $\rho_{c,rear}$, with a minimum allowed line width of 20 μm. The red star highlights the predicted efficiency corresponding to the best achieved recombination parameters for the laser doped contacts in this work. (For interpretation of the references to colour in this figure legend, the reader is referred to the Web version of this article.)

analysis from Quokka3 shows that recombination losses at the rear side constitute only a small fraction (~16%) of the total losses in this device, indicating that the PO_x/Al_2O_3-passivated and laser-doped rear is still not the limiting factor for efficiency. Additional reductions in rear side losses would be possible by moving to laser-doped point contacts in order to further reduce the rear contact fraction. Future work will therefore investigate J_0 and contact resistivity of laser-doped point-contact structures, and the implementation of such point contacts into proof-of-concept devices.

It is worth noting that the expected total area-weighted J_0 of the proposed rear structure based on PO_x/Al_2O_3 passivation with local laser-doped contacts is comparable to that expected for industrial $n+$ poly-Si/SiO_x passivated contact structures (for example, the parameters given in Ref. [43] for the latter imply a total J_0 of 10.8 fA cm^{-2}). However, the approach of this work offers potential advantages including i) lower thermal budget, ii) reduced optical losses in the infrared due to parasitic absorption by the rear poly-Si, and iii) improved bifaciality due to reduced absorption in the rear passivation stack.

4. Conclusions

PO_x/Al_2O_3 stacks have previously been shown to provide outstanding passivation of n-type silicon surfaces thanks to an exceptionally large positive fixed charge, making them highly promising for surface passivation applications. We have now demonstrated that the same stacks can provide additional functionality through their ability to be used as dopant sources for local contact formation via laser-doping. Specifically, we have demonstrated effective $n+$ laser doping from highly passivating PO_x/Al_2O_3 dielectric stacks using a pulsed nanosecond laser. Sheet resistances as low as 35 Ω/□ and surface dopant concentrations well above 10^{20} cm^{-3} were obtained for laser-doped regions. In the best case, we achieved a J_0 of 540 fA cm^{-2} for a metallised laser-doped region processed from a PO_x/Al_2O_3 stack providing J_0 of 2.5 fA cm^{-2} on undiffused planar n-type surfaces. This is on par with results for furnace diffusions at the same sheet resistance, indicating minimal additional defect generation resulting from laser processing. The combination of outstanding n-type surface passivation provided by such PO_x/Al_2O_3 stacks with local, self-aligned, laser-doped $n+$ contacts has the potential to substantially improve performance and simplify processing of high-efficiency silicon solar cells. As a specific example, we show through Quokka3 modelling that an efficiency of 23.6% can be achieved for commercial n-type front-emitter PERT/PERL cells by applying PO_x/Al_2O_3 as rear passivation and using laser-doping to form locally-diffused line contacts, when implemented together with previously roadmapped improvements to front-side passivation and extrinsic bulk lifetime.

Funding

This work was supported by the Australian Renewable Energy Agency (ARENA) through project RND017. Work at TU Eindhoven was supported by the Top consortia for Knowledge and Innovation Solar Energy program "RADAR" of the Ministry of Economic Affairs of The Netherlands. The work of J. Melskens was supported by the Netherlands Organisation for Scientific Research under the Dutch TTW-VENI Grant 15896.

CRediT authorship contribution statement

Lachlan E. Black: Conceptualization, Methodology, Investigation, Visualization, Writing - original draft. **Marco Ernst:** Conceptualization, Methodology, Investigation, Visualization, Writing - review & editing. **Roel Theeuwes:** Investigation, Writing - review & editing. **Jimmy Melskens:** Investigation, Writing - review & editing. **Daniel Macdonald:** Writing - review & editing, Supervision, Funding acquisition. **W.M. M.(Erwin) Kessels:** Writing - review & editing, Supervision, Funding acquisition.

Declaration of competing interest

The authors declare that they have no known competing financial interests or personal relationships that could have appeared to influence the work reported in this paper.

Acknowledgements

The authors thank D. Walter (ANU) for advice regarding the deconvolution of the PL images, S. Surve (ANU) for assistance with ECV measurements, and B. Macco (TU/e) for feedback on the draft manuscript.

References

[1] J. Zhao, A. Wang, P. Altermatt, M.A. Green, Twenty-four percent efficient silicon solar cells with double layer antireflection coatings and reduced resistance loss, Appl. Phys. Lett. 66 (26) (1995) 3636–3638.
[2] E. Franklin, K. Fong, K. McIntosh, A. Fell, A. Blakers, T. Kho, D. Walter, D. Wang, N. Zin, M. Stocks, E.-C. Wang, N. Grant, Y. Wan, Y. Yang, X. Zhang, Z. Feng, P. J. Verlinden, Design, fabrication and characterisation of a 24.4% efficient interdigitated back contact solar cell, Prog. Photovoltaics Res. Appl. 24 (4) (2014) 411–427.
[3] M. Dahlinger, K. Carstens, E. Hoffmann, S. Wansleben, J.R. Köhler, R. Zapf-Gottwick, J.H. Werner, 23.3% efficiency with laser processed IBC solar cells,, in: Proc. 31st European Photovoltaic Solar Energy Conference, 2015, pp. 462–465.
[4] M. Ernst, E. Franklin, A. Fell, K. Fong, D. Walter, E.-C. Wang, T. Kho, A. Blakers, Fabrication of a 22.8% efficient back contact solar cell with localized laser-doping, Phys. Status Solidi 214 (11) (2017), 1700318.
[5] T. Dullweber, J. Schmidt, "Industrial silicon solar cells applying the passivated emitter and rear cell (PERC) concept—a review, IEEE J. Photovoltaics 6 (5) (Sep. 2016) 1366–1381.
[6] J. Weber, S. Gutscher, S. Lohmüller, E. Lohmüller, A.A. Brand, Laser-doped selective emitter - process development and speed-up, in: Proc. 35th Eur. Photovolt. Sol. Energy Conf. Exhib, 2018, pp. 379–384.
[7] T. Röder, P. Grabitz, S. Eisele, C. Wagner, J.R. Köhler, J.H. Werner, 0.4% absolute efficiency gain of industrial solar cells by laser doped selective emitter, in: 2009 34th IEEE Photovoltaic Specialists Conference (PVSC), June 2009, pp. 871–873.
[8] U. Jäger, M. Okanovic, M. Hörteis, A. Grohe, R. Preu, Selective emitter by laser doping from phosphosilicate glass, in: Proc. 24th European Photovoltaic Solar Energy Conference, 2009, pp. 1740–1743.
[9] C. Duran, S.J. Eisele, T. Buck, R. Kopecek, J.R. Köhler, J.H. Werner, Bifacial solar cells with selective B-BSF by laser doping, in: 24th European Photovoltaic Solar Energy Conference, 2009, pp. 21–25.
[10] M. Heilig, J. Engelhardt, G. Hahn, B. Terheiden, Comparison of laser-doped emitters from as-deposited and thermally diffused APCVD doping glasses on silicon substrates, AIP Conference Proceedings 2147 (1) (2019), 070004.
[11] P. Prathap, J. Bartringer, A. Slaoui, Selective emitter formation by laser doping of spin-on sources, Appl. Surf. Sci. 278 (2013) 173–179.
[12] M. Ernst, A. Fell, E. Franklin, K.J. Weber, Characterization of recombination properties and contact resistivity of laser-processed localized contacts from doped silicon nanoparticle ink and spin-on dopants, IEEE J. Photovoltaics 7 (2) (March 2017) 471–478.
[13] A. Fell, E. Franklin, D. Walter, D. Suh, K. Weber, Laser doping from Al_2O_3 layers, in: Proc. 27th European Photovoltaic Solar Energy Con., 2012, pp. 706–708.
[14] D. Walter, A. Fell, M. Ernst, E. Franklin, K. Weber, Electronic properties of Al p+ surfaces formed by laser doping from aluminium oxide precursors: implications for PERC cell design and performance, Energy Procedia 77 (2015) 321–330.
[15] E. Cornagliotti, A. Uruena, B. Hallam, L. Tous, R. Russell, F. Duerinckx, J. Szlufcik, Large area p-type perl cells featuring local p+ BSF formed by laser processing of ALD Al_2O_3 layers, Sol. Energy Mater. Sol. Cell. 138 (2015) 72–79.
[16] N.-P. Harder, Y. Larionova, R. Brendel, Al+-doping of Si by laser ablation of Al_2O_3/SiN passivation, Phys. Status Solidi 210 (9) (2013) 1871–1873.
[17] M. Ernst, D. Walter, A. Fell, B. Lim, K. Weber, Efficiency potential of p-type Al_2O_3/SiN_x passivated PERC solar cells with locally laser-doped rear contacts, IEEE J. Photovoltaics 6 (3) (May 2016) 624–631.
[18] I. Martín, P. Ortega, M. Colina, A. Orpella, G. López, R. Alcubilla, Laser processing of Al_2O_3/a-SiC_x:H stacks: a feasible solution for the rear surface of high-efficiency p-type c-Si solar cells, Prog. Photovoltaics Res. Appl. 21 (5) (2013) 1171–1175.
[19] P. Ortega, I. Martín, G. Lopez, M. Colina, A. Orpella, C. Voz, R. Alcubilla, p-type c-Si solar cells based on rear side laser processing of Al_2O_3/SiC_x stacks, Sol. Energy Mater. Sol. Cell. 106 (2012) 80–83.
[20] T.G. Allen, M. Ernst, C. Samundsett, A. Cuevas, Demonstration of c-Si solar cells with gallium oxide surface passivation and laser-doped gallium p+ regions, IEEE J. Photovoltaics 5 (6) (Nov 2015) 1586–1590.
[21] B. Steinhauser, U. Jäger, J. Benick, M. Hermle, PassDop rear side passivation based on Al_2O_3/a-SiC_x:B stacks for p-type PERL solar cells, Sol. Energy Mater. Sol. Cell. 131 (2014) 129–133.
[22] S. Gall, B. Paviet-Salomon, J. Lerat, T. Emeraud, High quality passivation scheme combined with laser doping from SiN:P and SiN:B layer for silicon solar cell, Energy Procedia 27 (2012) 467–473.
[23] M.H. Norouzi, P. Saint-Cast, U. Jaeger, B. Steinhauser, J. Benick, A. Buechler, B. Bitnar, P. Palinginis, H. Neuhaus, A. Wolf, M. Hofmann, Development and characterization of AlO_x/SiN_x:B layer systems for surface passivation and local laser doping, IEEE J. Photovoltaics 7 (5) (Sep. 2017) 1244–1253.
[24] U. Jäger, D. Suwito, J. Benick, S. Janz, R. Preu, A laser based process for the formation of a local back surface field for n-type silicon solar cells, Thin Solid Films 519 (11) (2011) 3827–3830.
[25] D. Suwito, U. Jäger, J. Benick, S. Janz, M. Hermle, S.W. Glunz, Industrially feasible rear passivation and contacting scheme for high-efficiency n-type solar cells yielding a V_{oc} of 700 mV, IEEE Trans. Electron. Dev. 57 (8) (Aug 2010) 2032–2036.
[26] B. Paviet-Salomon, S. Gall, R. Monna, S. Manuel, A. Slaoui, L. Vandroux, R. Hida, S. Dechenaux, Laser doping using phosphorus-doped silicon nitrides, Energy Procedia 8 (2011) 700–705.
[27] B. Steinhauser, M. bin Mansoor, U. Jäger, J. Benick, M. Hermle, Firing-stable PassDop passivation for screen printed n-type PERL solar cells based on a-SiN_x:P, Sol. Energy Mater. Sol. Cell. 126 (2014) 96–100.
[28] L.E. Black, W.M.M. Kessels, PO_x/Al_2O_3 stacks: highly effective surface passivation of crystalline silicon with a large positive fixed charge, Appl. Phys. Lett. 112 (20) (2018), 201603.
[29] L.E. Black, W.M.M. Kessels, Investigation of crystalline silicon surface passivation by positively charged PO_x/Al_2O_3 stacks, Sol. Energy Mater. Sol. Cell. 185 (2018) 385–391.
[30] J. Melskens, R.J. Theeuwes, L.E. Black, W.-J.H. Berghuis, B. Macco, P.C. P. Bronsveld, E.W.M.M. Kessels, Outstanding Passivation of n-type Silicon Surfaces Enabled by Pulsed-Flow Plasma-Enhanced Chemical Vapor Deposition of Phosphorus Oxide Capped by Aluminum Oxide, 2020 forthcoming.
[31] F.M. Smits, Measurement of sheet resistivities with the four-point probe, Bell Syst. Techn. J. 37 (3) (1958) 711–718.
[32] D. Walter, A. Fell, E. Franklin, D. Macdonald, B. Mitchell, T. Trupke, The impact of silicon CCD photon spread on quantitative analyses of luminescence images, IEEE J. Photovoltaics 4 (1) (Jan 2014) 368–373.
[33] D. Sage, L. Donati, F. Soulez, D. Fortun, G. Schmit, A. Seitz, R. Guiet, C. Vonesch, M. Unser, DeconvolutionLab2: an open-source software for deconvolution microscopy, Methods 115 (2017) 28–41.
[34] L.E. Black, D.H. Macdonald, Accounting for the dependence of coil sensitivity on sample thickness and lift-off in inductively coupled photoconductance measurements, IEEE J. Photovoltaics 9 (6) (Nov 2019) 1563–1574.
[35] D.E. Kane, R.M. Swanson, Measurement of the emitter saturation current by a contactless photoconductivity decay method, in: Conf. Rec. 18th IEEE Photovoltaic Specialists Conf, Las Vegas, USA, 21 October 1985, pp. 578–583.
[36] A. Richter, S.W. Glunz, F. Werner, J. Schmidt, A. Cuevas, Improved quantitative description of Auger recombination in crystalline silicon, Phys. Rev. B 86 (2012).
[37] A.B. Sproul, M.A. Green, Improved value for the silicon intrinsic carrier concentration from 275 to 375 K, J. Appl. Phys. 70 (2) (1991) 846–854.
[38] D. Walter, A. Liu, E. Franklin, D. Macdonald, B. Mitchell, T. Trupke, Contrast enhancement of luminescence images via point-spread deconvolution, in: Proc. 38th IEEE Photovoltaic Specialists Conference, June 2012, pp. 307–312.
[39] D. Yan, A. Cuevas, Empirical determination of the energy band gap narrowing in highly doped n+ silicon, J. Appl. Phys. 114 (4) (2013).
[40] A. Fell, J. Schön, M.C. Schubert, S.W. Glunz, The concept of skins for silicon solar cell modeling, Sol. Energy Mater. Sol. Cell. 173 (2017) 128–133.
[41] J. Rodriguez, E.-C. Wang, N. Chen, J.W. Ho, M. Li, J.K. Buatis, B. Nagarajan, L. Xu, W.L. Choy, V. Shanmugam, J. Wong, A.G. Aberle, S. Duttagupta, Towards 22% efficient screen-printed bifacial n-type silicon solar cells, Sol. Energy Mater. Sol. Cell. 187 (2018) 91–96.
[42] C. Comparotto, J. Lossen, V.D. Mihailetchi, Bifacial screen-printed n-type passivated emitter rear totally diffused rear junction solar cells, AIP Conference Proceedings 1999 (1) (2018), 100001.
[43] L. Tous, P. Choulat, S. Singh, J. John, M. Aleman, M. Firat, F. Duerinckx, J. Szlufcik, Efficiency roadmaps for industrial bifacial pPERC and nPERT cells, AIP Conference Proceedings 2147 (1) (2019), 120001.
[44] K.R. McIntosh, P.P. Altermatt, A freeware 1D emitter model for silicon solar cells, in: Proc. 35th IEEE Photovoltaic Specialists Conference, June 2010, pp. 2188–2193.
[45] M. Ernst, J.D. Huyeng, D. Walter, K.C. Fong, A. Blakers, Unravelling the origins of contact recombination for localized laser-doped contacts, in: Proc. 7th World Conf. Photovoltaic Energy Conversion (WCPEC), June 2018, pp. 2195–2199.